www.elsevier.com/locate/memsci

Extending Effective Medium Theory to Finite Size Systems: Theory and Simulation for Permeation in Mixed-Matrix Membranes

Gloria M. Monsalve-Bravo, Suresh K. Bhatia

PII: S0376-7388(16)32493-0
DOI: http://dx.doi.org/10.1016/j.memsci.2017.02.029
Reference: MEMSCI15088

To appear in: *Journal of Membrane Science*

Received date: 9 December 2016
Accepted date: 7 February 2017

Cite this article as: Gloria M. Monsalve-Bravo and Suresh K. Bhatia, Extendin Effective Medium Theory to Finite Size Systems: Theory and Simulation fo Permeation in Mixed-Matrix Membranes, *Journal of Membrane Science* http://dx.doi.org/10.1016/j.memsci.2017.02.029

Extending Effective Medium Theory to Finite Size Systems: Theory and Simulation for Permeation in Mixed-Matrix Membranes

Gloria M. Monsalve-Bravo, Suresh K. Bhatia*

School of Chemical Engineering, The University of Queensland, Brisbane QLD 4072, Australia

*Corresponding author. Email address: s.bhatia@uq.edu.au (S.K. Bhatia)

Abstract

We present a novel theory for estimation of the effective permeability of pure gases in flat mixed-matrix membranes (MMMs), in which effective medium theory (EMT) is extended to systems with finite filler size and membrane thickness. We introduce an inhomogeneous filler volume fraction profile, which arises due to depletion of the filler in regions adjacent to the membrane ends, into the MMM permeation model. In this way, the effective medium approach (EMA) can still be applied to systems where the dispersant size is not small in comparison to the membrane thickness, and for which a permeability profile arises in th MMM that is dependent on both filler size and membrane thickness, besides the filler-polymer equilibrium constant. It is found that increase in particle size reduces the effective membrane permeability at fixed membrane thickness, and that the effective membrane permeability increases with increase of the membrane thickness to asymptotically reach the value predicted by existing models. The present theory is validated against detailed simulations of the transport in MMMs, and theoretical predictions are found to be in agreement with those obtained from the exact calculations. Further, comparison of the exact effective permeability at different filler volume fractions is made for different packing configurations, showing variations in dispersant packing structure to have only a very weak effect on MMM performance.

Graphical abstract

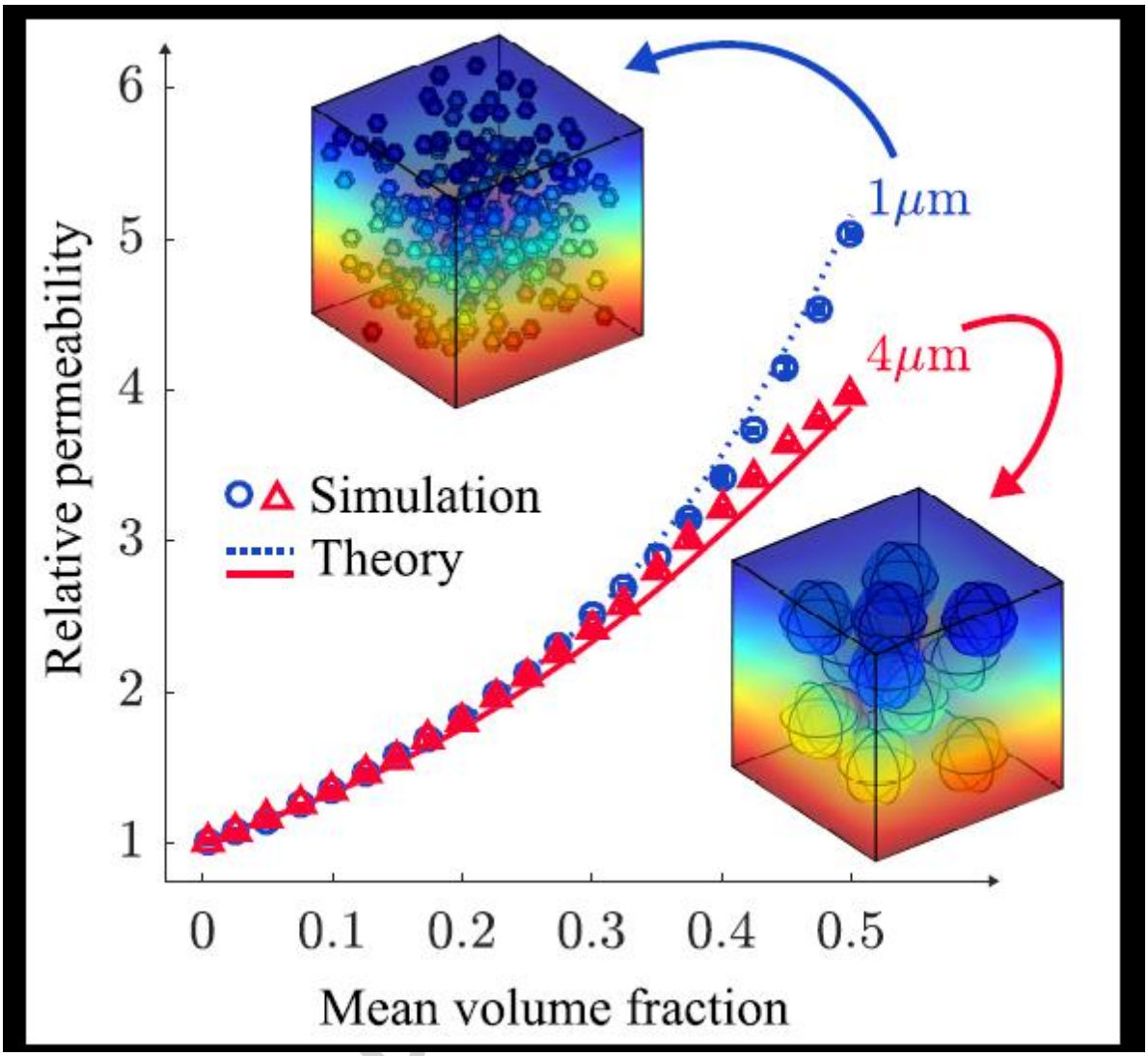

Keywords: Permeation in mixed-matrix membranes, effective permeability, effective medium theory, finite size systems, simulation of transport in mixed matrix membranes

1. Introduction

Materials chemistry and structure play a critical role in the attainment of high membrane permeability and selectivity [1–3]. Based on their materials, membranes can be classified into two major groups: (i) polymeric or (ii) inorganic [1,4], of which the former type is known to have a wide range of molecular transport properties, easy processing techniques, high mechanical stability, and low manufacturing costs [5,6]. However, they fail to overcome the

well-known permeability-selectivity upper bound (also known as Robeson's upper bound) [1,7,8]. Inorganic membranes, on other hand, offer higher permeability and selectivity than polymeric membranes, but their applications are limited by their fragility and higher cost over organic membranes [9,10]. Because achieving both high gas permeability and selectivity is desirable, the synthesis of membranes performing beyond Robeson's upper bound has been the focus of multiple studies [3,4,11–13], in which mixed-matrix membranes (MMMs) have become a fast growing branch of membrane-based separation technologies [1,6,14]. MMMs are hybrid composite membranes containing inorganic filler particles (e.g. zeolites, metal organic framework materials or activated carbon) dispersed in a continuous organic (polymer) matrix [4,5,15]. Such composite membranes are cost-effective, mechanically resistant and, thermally and chemically robust while offering high selectivity and permeability [6,7,10], thereby providing the advantages of both types of conventional membranes.

Notwithstanding the benefits of MMM-based separation processes, there are still obstacles that need to be addressed for optimization of their industrial implementation [8]. A key challenge is the necessity of characterizing the transport of species across the membrane and its dependence on inherent filler-matrix properties [6,16,17]. Current research is centered on the determination of a suitable pair combination of polymer and filler phases [13,18], the impact of membrane geometry on separation efficiency [1,4,15], the effect of dispersant physical properties (i.e. particle size, shape and distribution) [19–21], and the influence of polymer-particle interfacial morphologies [6,13,22]. Although much effort has been devoted to mathematically representing such effects [13,16,17], existing models are adaptations of highly idealised early theories of transport in composite materials [13,22–29] while considering a linear concentration profile and empirically embedding the effects of filler properties in a single parameter (maximum filler volume fraction) [6,30]. Such an approach masks the effect of nonuniformity of the concentration field and its interplay with dispersant size on the composite membrane performance.

Current permeation models often treat the heterogeneous membrane under the restriction that one of the phases is finely dispersed in the other, so that the composite can be considered macroscopically homogeneous [25,31,32]. However, when the ratio of the membrane thickness to the filler size is not very large, EMT-based models are unable to quantitatively estimate the

MMM permeability [5,15,33,34]. Here, we present a model for the permeation of pure gases in MMMs, explicitly considering the effect of filler size of filler and membrane thickness, and the interplay with the interfacial adsorption equilibrium, overcoming the assumption of uniformity of the field (e.g. potential gradient in electric conduction, and pseudo-bulk concentration or pressure gradient in MMM permeation), inherent to existing models of transport in composite media. To validate the proposed theory, rigorous 3d simulations of the diffusive transport in MMMs have been performed, in which the simulation results are considered to be the exact solution to the transport problem in the MMMs. Further, five different packing configurations (i.e. random, simple cubic, body-centered cubic, face-centered cubic and hexagonal close-packed structures) and dispersant sizes are considered, for which the variation of MMM permeability with filler volume fraction is determined and compared.

2. Permeation models for composite membranes

Although there exist a plethora of models to predict the permeation properties of MMMs [9,13,16,17,22–25,27–30,35–39], most are adaptations of highly idealized early theories of conduction in composite materials falling within the scope of effective medium theory (EMT) [13,22–29]. The crux of EMT is the substitution of a given composite system by an equivalent effective homogeneous one with the properties of the dispersion [31,40]. In general, permeation models consider either a low filler volume fraction or a small difference between the permeabilities of the filler and matrix [23,35,40,41]. Among the most significant results within the first group is that of Jeffrey [24,42], who showed that the relative permeability $\left(P_r\right)$ can be expanded in a series of the form [43]:

$$P_r = \frac{P_m}{P_c} = 1 + K_1\phi_o + K_2\phi_o^2 + \cdots \tag{1}$$

where P_m and P_c denote the permeabilities of the MMM and continuous phase, respectively. Here, ϕ_o represents the nomimal dispersant volume fraction, which is commonly assumed to be uniform. Each term in the expansion $\left(K_1, K_2, \ldots, K_n\right)$ takes into account the interaction between successively larger sets of particles [24,42]. Existing models are then simplifications or

adaptations of Eq. (1) [13,22–29]. The most popular ones are summarized in Table 1, highlighting their key features. All of these consider spherical filler particles as inclusions.

Table 1. Summary of most popular permeation models.

Model	Equation	Large permeability differences	High filler loadings	Filler morphology
Maxwell [26]	$P_r = \frac{1+2\beta\phi_o}{1-\beta\phi_o}$	✗	✗	✗
Chiew–Glandt [23]	$P_r = \frac{1+2\beta\phi_o+(K_2-3\beta^2)\phi_o^2}{1-\beta\phi_o}$	✓	✓	✗
Lewis–Nielsen [38]	$P_r = \frac{1+A\beta\phi_o}{1-\beta\phi_o\psi_m}$	✓	✓	✓
Bruggeman [44]	$P_r^{\frac{1}{3}}\left[\frac{\alpha-1}{\alpha-P_r}\right] = \left[1-\phi_o\right]^{-1}$	✗	✓	✗
Pal [25]	$P_r^{\frac{1}{3}}\left[\frac{\alpha-1}{\alpha-P_r}\right] = \left[1-\frac{\phi_o}{\phi_m}\right]^{-\phi_m}$	✗	✓	✓

Among the models in Table 1, that of Maxwell [26] was developed for the effective electrical conductivity of a dilute dispersion of particles in an infinite matrix using an effective medium approach (EMA) [6,23,26,35,45]. Only the first-order term of the Maxwell model is exact, i.e.

$$P_r = 1+3\beta\phi_o+\mathcal{O}\left(\phi_o^2\right) \tag{2}$$

with β given by [23,24,42]:

$$\beta = \left(\frac{\alpha - 1}{\alpha + 2} \right) \tag{3}$$

where $\alpha = P_f / P_c$ is the ratio of the permeability of the dispersed to the continuous phase. Since the Maxwell model disregards interaction between particles, it generally describes the permeability well only at low loadings of filler particles with $\phi_o \leq 0.2$ [2,6,14,46]. Furthermore, the Maxwell model is the simplest among the various models presented in Table 1, and considers dispersant particle size to be negligibly small with no aggregation [2,17,30,35,46].

Chiew and Glandt [23] extended Jeffrey's model to higher particle concentrations [43], using pair-correlation functions of hard-sphere fluids in the equilibrium state [23,47] to replace the probability calculation based on well-stirred distributions [24,42]. Such modification led to the appropriate estimation of K_2 in Eq. (1), in which the series simplifies to yield the Chiew-Glandt model in Table 1 [6,48]. The resulting values of K_2 were tabulated as function of α and ϕ_o. Later, Gonzo et al. [35] fitted Chiew and Glandt's results for K_2 to the following expressions:

$$K_2 = a + b\phi_o^{\frac{3}{2}} \tag{4}$$

$$a = -0.002254 - 0.123112\beta + 2.93656\beta^2 + 1.6904\beta^3 \tag{5}$$

$$b = 0.0039298 - 0.803494\beta - 2.16207\beta^2 + 6.48296\beta^3 + 5.27196\beta^4 \tag{6}$$

Although the Chiew-Glandt model may be applicable to moderate particle concentration [23], the effect of filler properties such as particle size and morphology remains to be considered.

Lewis and Nielsen [38] extended the Halpin-Tsai equation, originally developed for the elastic modulus of particulate composites, to the thermal conductivity of heterogeneous media [29,49]. In their result, presented in Table 1, the value of the parameter ψ_m depends on the maximum filler volume fraction in the system (ϕ_m) and is given by:

$$\psi_m = 1 + \left(\frac{1 - \phi_m}{\phi_m^2} \right) \phi_o \tag{7}$$

Further, in the Lewis-Nielsen model in Table 1, $A = k_E - 1$ and is a constant related to the filler shape depending on the Einstein coefficient (k_E). For a suspension of rigid spheres $k_E = 2.5$, so that $A = 1.5$ [28,29]. Later, Pal [27] proposed that for spherical particles, A should take the value of 2 instead of 1.5 to allow the Lewis-Nielsen model to be consistently simplified into the Maxwell model when $\phi_m \to 1$.

The Bruggeman model was originally developed for the dielectric constant of particulate composites using differential effective medium theory (DEMT) [6,9,25,44], which builds up a composite medium through a process of incremental homogenization [31,35]. The approach proceeds from the premise that the fields of neighboring particles can be taken into account by adding the dispersed particles incrementally while considering the surrounding medium as the existing composite at each stage [31,41,50]. Thus, assuming that Maxwell's equation is a good enough approximation to characterize suspensions with low particle concentrations, Bruggeman [44] established an expression for the increment on the thermal conductivity due to infinitesimal increments in the filler loading. Such increment dP resulting from the addition of new particles may be obtained calculated from Eq. (2) by substituting $P_c \to P$, $P_m \to P + dP$ and $\phi_o \to d\phi_o/(1-\phi_o)$, which, after integration, leads to the Bruggeman model in Table 1.

The Pal model was originally developed for thermal conductivity of particulate composites [6,25,27], in an manner analogous to that of Bruggeman [44] and also under the scope of the DEMT. He derived an expression for the infinitesimal increment of the dispersion conductivity while introducing the volume fraction dependence on the maximum filler packing fraction (ϕ_m). Such increment dP resulting from the addition of new particles was also calculated from Eq. (2) substituting $P_c \to P$ and $P_m \to P + dP$ but $\phi_o \to d\phi_o/(1-\phi_o/\phi_m)$ instead of $\phi_o \to d\phi_o/(1-\phi_o)$, which, after integration, leads to the Pal model in Table 1 [35]. Bruggeman's result is a special case of the Pal model for $\phi_m = 1$, whence the two become identical.

Among the limitations of the above-described models, the most significant ones are the assumption of uniform concentration field together with the consideration of an infinite system [5,9,51]. Such assumptions make the permeability independent of the membrane thickness and

particle size. Futhermore, the effect of filler properties including particle size is embedded in a single empirical morphology-related parameter, such as in the Pal [25] and Lewis-Nielsen [38] models. Further, permeation models often cannot match or reconcile experimental data without the postulation of nonidealities, such as the presence of interfacial voids [13,52] or rigidified polymeric regions at the interface with the filler [22,30,53,54]. Such nonidealities are typically taken into account by modifying EMT-based models to include ispecific interfacial regions at the filler- matrix interface. Here, because DEMT treats local variations in the system as fluctuations in an effective unvarying medium, no discrimination between both continuous and suspended phases is made [35]. Thus, no information on the system morphology can be obtained from the model [2,30,43].

Although much effort has been devoted to the improvement of EMT models, their limitations have prompted reserachers to explore more accurate approaches such as the detailed simulation of MMMs [15,55–57], in which the coupled 3d transport equations for the transport in the filler particles and in the surrounding polymer matrix are simultaneously solved using the finite element method (FEM). Such detailed 3d simulation overcomes limitations of EMT models in the estimation of the effective permeability, particularly the effect of particle size and the interfacial adsorption equilibrium [5]. Moreover, detailed simulation is able to embrace large differences among the Fickian diffusivities in both phases, and their interplay with particle size effects as well as permeant concentration inhomogeneities due to particle interaction [58].

Recently, Singh et al. [5] performed simulations of the transport in 3d-MMMs with randomly distributed spherical fillers, using the COMSOL multiphysics software package [59], and estimated the relative permeability $\left(P_r = P_m / P_c\right)$ as function of the filler volume fraction. They used the adsorbed concentration as field variable, with a linear isotherm in each phase, so that the equilibrium constant was defined as the ratio between the adsorbed concentration in the filler to that in the polymer, i.e. $K_f / K_c = q_f / q_c$, where q_f and q_c are the adsorbed concentrations in the filler and polymer phases, respectively, and K_f, K_c are the corresponding gas-solid equilibrium constants. In this manner, they were able to estimate the relative permeability as the ratio of the fluxes in the permeate direction of the MMM to that in the corresponding polymer matrix. Their predictions showed that the various permeation models, given in Table 1, are

unable to address the dependence of relative permeability on the equilibrium constant. Besides, they also studied the effect of particle size on the MMM performance; however, the relative permeability was found to be independent of the particle size in the range of sizes investigated.

Subsequently, Yang et al. [15], following the same approach as Singh et al. [5], calculated the relative permeability of 3d hollow-fiber and dense flat MMMs, also with randomly distributed spherical fillers. They studied the effects of filler-to-matrix self-diffusivity ratio $\left(\mathcal{D}_{of}/\mathcal{D}_{oc}\right)$, filler-to-matrix equilibrium constant ratio $\left(K_f/K_c = q_f/q_c\right)$ and filler size on MMM performance, finding that in general hollow-fibers had higher effective permeabilities than flat-dense MMMs. Nevertheless, in contrast with Singh et al. [5], the relative permeability was found to increase with the decrease of the filler size for both flat-dense and hollow-fiber MMMs. Most likely, the discrepancy between the results of Singh et al. [5] and Yang et al. [15] is associated with the mesh quality used in FEM implementation, and issues related to numerical convergence [15]. Our simulations results address such issues, while investigating the effect of particle size and other system parameters, as described below.

3. Methods

3.1. Theory

3.1.1. Transport model

We consider a flat mixed matrix membrane of finite thickness ℓ, comprising uniformly sized spheres of radius r_o dispersed in a polymer matrix. Steady state transport through the mixed-matrix membrane is described by the continuity equation:

$$\frac{d}{dx}\left[\mathcal{D}_m(x)\frac{dC_b^m}{dx}\right] = 0 \tag{8}$$

in which we use the pseudo-bulk concentration $\left(C_b^m\right)$ in the mixed matrix as the field variable, with the following boundary conditions:

$$x = 0 \qquad C_b^m = C_{b2} \tag{9}$$

$$x = \ell \qquad C_b^m = C_{b1} \tag{10}$$

Here the local diffusivity of the mixed-matrix membrane $\left(\mathcal{D}_m\right)$ is estimated using a suitable EMT-based model, in which the filler $\left(\mathcal{D}_f\right)$ and matrix $\left(\mathcal{D}_c\right)$ local Fickian diffusivities follow the Darken relation, leading to

$$\mathcal{D}(C_b^m) = \mathcal{D}_o \frac{I(C_b^m)}{C_b^m} \tag{11}$$

where $\mathcal{D}_o$ is the mobility [60,61], and $I\left(C_b^m\right)$ the local adsorption isotherm, in any given phase (filler or matrix). Here, $\mathcal{D}_c$, $\mathcal{D}_f$ and $\mathcal{D}_m$ have similar connotation as permeability (P_c, P_f and P_m respectively), since we use the pseudo-bulk concentration as the field variable. The mixed-matrix permeability, $\mathcal{D}_m$, can be position-dependent, not only due to concentration dependence of the filler and polymer dffusivities, but also due to the presence of inhomogeneity in the filler volume fraction, discussed below. At low pressures, i.e. in the Henry's law region, the adsorbed gas concentration is given by:

$$I(C_b^m) = KC_b^m \tag{12}$$

and $\mathcal{D}_f$ and $\mathcal{D}_c$ then follow

$$\mathcal{D}_f = K_f \mathcal{D}_{of} \tag{13}$$

$$\mathcal{D}_c = K_c \mathcal{D}_{oc} \tag{14}$$

with K_f and K_c being the Henry's law constants for the filler and matrix, respectively. While the above approach is general, in the present work we will confine ourselves to the low pressure Henry law region.

3.1.2. Filler volume fraction profile

The filler volume fraction (ϕ_o) in the EMT models in Table 1, is commonly considered to be homogeneous and uniform due to the underlying assumption of the system effectively being an infinitely large continuum. Such an assumption precludes end effects that will arise in a finite system, in which there will be regions near the surface, of thickness equal to the particle radius, in which no particle centres can lie. Thus, if a finite membrane of thickness ℓ containing spherical particles of radius r_o is considered, as shown in Fig. 1, there can be no particle centres in the regions $0 < x < r_o$ and $\ell - r_o < x < \ell$, and only portions of spheres can occupy these regions. Consequently, the filler volume fraction will be smaller than ϕ_o in these regions. Similarly, the absence of sphere centres in these end regions implies that the filler volume fraction in their neighbouring regions $\ell - r_o < x < \ell - 2r_o$ and $r_o < x < 2r_o$ will also be less than ϕ_o. This leads to a profile of the filler volume fraction as a function of position within the membrane.

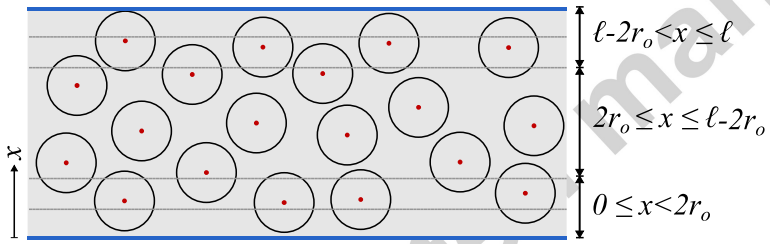

Fig. 1. Variation of filler volume fraction with position for $\ell \geq 4r_o$.

As a first approximation, we may assume the EMT to be applicable at any position in the membrane, with the corresponding effective permeability evaluated at the local filler volume density. The motivation for this approach follows from the work of Chang and Acrivos [33], who found such an assumption to be successful in the context of heat transfer from a planar wall to a dispersion of finite size spheres in a continuous matrix. To derive an expresion for the filler volume fraction profile, we consider the differential volume in the region $[x, x+dx]$ of a sphere centred at position x' within the membrane:

$$dV = \pi\left[r_o^2 - (x'-x)^2\right]dx, \quad |x'-x| < r_o, \quad 0 < x < r_o \tag{15}$$

Here, x is the distance from one side of the membrane measured along the normal to the surface. Considering a differential portion of the membrane in $\left[x', x'+dx'\right]$ with volume Adx' and having $NAdx'$ particle centers, where A is the membrane cross-sectional area on the yz-plane and N the particle number density (assumed uniform), the differential filler volume fraction in $\left[x, x+dx\right]$ is given as:

$$d\phi = \frac{NAdx'}{Adx}\pi\left[r_o^2 - \left(x'-x\right)^2\right]dx \tag{16}$$

On defining the nominal filler volume fraction as $\phi_o = \frac{4}{3}N\pi r_o^3$, Eq. (16) may be rewritten as:

$$d\phi = \frac{3\phi_o}{4r_o^3}\left[r_o^2 - \left(x'-x\right)^2\right]dx' \tag{17}$$

and for particles located in $0 \le x < 2r_o$, the volume fraction is given by (c.f. Fig. 1):

$$\phi\left(x\right) = \frac{3\phi_o}{4r_o^3}\int_{r_o}^{r_o+x}\left[r_o^2 - \left(x'-x\right)^2\right]dx' \tag{18}$$

Similarly, for particles located in $\ell - 2r_o < x \le \ell$, the volume fraction is given by (c.f. Fig. 1):

$$\phi\left(x\right) = \frac{3\phi_o}{4r_o^3}\int_{x-r_o}^{\ell-r_o}\left[r_o^2 - \left(x'-x\right)^2\right]dx' \tag{19}$$

Upon performing the integrations in Eqs. (18) and (19), the filler volume fraction profile is obtained as:

$$\phi(x) = \begin{cases} \dfrac{\phi_o}{4r_o^3}x^2\left(3r_o - x\right) & 0 \le x < 2r_o \\ \phi_o & 2r_o \le x \le \ell - 2r_o \\ \dfrac{\phi_o}{4r_o^3}\left(\ell - x\right)^2\left[3r_o - \left(\ell - x\right)\right] & \ell - 2r_o < x \le \ell \end{cases} \tag{20}$$

where Eq. (20) is applicable to flat MMMs for which $\ell \geq 4r_o$. The above volume fraction profile agrees with Eq. (9) of Ref. [33], for both membrane ends. Eqs. (18) and (19) hold for both membrane ends even for MMM in which $2r_o \leq \ell \leq 4r_o$. However, for such MMMs the filler volume fraction is no longer uniform in the internal region $\ell - 2r_o \leq x \leq 2r_o$, since the filler depletion also extends into this region, as shown in Fig. 2.

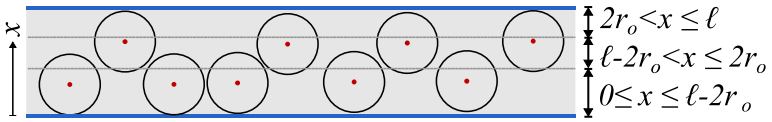

Fig. 2. Variation of filler volume fraction with position for $2r_o \leq \ell \leq 4r_o$.

Thus, for particles located in $\ell - 2r_o \leq x \leq 2r_o$, the volume fraction is given by:

$$\phi(x) = \frac{3\phi_o}{4r_o^3} \int_{r_o}^{\ell - r_o} \left[r_o^2 - (x' - x)^2 \right] dx' \tag{21}$$

which after integration leads to

$$\phi = \begin{cases} \dfrac{\phi_o}{4r_o^3} x^2 (3r_o - x) & 0 \leq x \leq \ell - 2r_o \\ \dfrac{\phi_o}{4r_o^3} (\ell - 2r_o)\left(2r_o^2 + r_o\ell - \ell^2 + 3\ell x - 3x^2\right) & \ell - 2r_o < x \leq 2r_o \\ \dfrac{\phi_o}{4r_o^3} (\ell - x)^2 \left[3r_o - (\ell - x)\right] & 2r_o < x \leq \ell \end{cases} \tag{22}$$

Further, $\phi(x) = 0$ for membranes for which $\ell \leq 2r_o$. The ratio, $\phi(x)/\phi_o$ represents the probability that a given point in the composite lies within a sphere [34] . Upon integration of the profiles in Eqs. (20) and (22), the mean filler volume fraction is obtained as:

$$\langle \phi \rangle = \frac{\int_0^\ell \phi(x) dx}{\int_0^\ell dx} = \frac{\phi_o}{\ell} (\ell - 2r_o) \tag{23}$$

in which the second term within the parenthesis represents the effect of the two exclusion regions of thickness r_o on each side of the membrane, where no particle centres can lie.

The use of EMT with the above local filler volume fraction profile, i.e. with $\mathcal{D}_m$ evaluated using $\phi(x)$ to replace ϕ_o in any of the models in Table 1, is at best a first approximation, as it does not consider the variation of filler volume fraction in the space occupied by the particle. Such nonlocal effects lead to variation of the effective permeability at the scale of the dipersant particles, and are most conveniently captured by the local average density model (LADM), first proposed by Bitsanis et al. [62,63] in modeling the position-dependent viscosity of an inhomogeneous fluid. The LADM volume averages the position-dependent number density of particle centres over the space occupied by a single particle, and evaluates the local transport property at this locally volume-averaged density. The LADM has also found success in our group in modeling the transport of adsorbates in nanopores [64,65], where strong inhomogeneities exist. In the present context, since the local number density of particle centres is proportional to the local filler volume fraction, we appeal to th LADM and incorporate nonlocal effects through the average of the filler volume fraction profile over the volume of a single filler particle, i.e.

$$\bar{\phi}(x) = \frac{3}{2r_o^3}\int_0^{r_o}\int_0^{\pi} \phi(x + r\cos\theta) r^2 \sin\theta \, d\theta \, dr \tag{24}$$

where $\bar{\phi}(x)$ is a coarse-grained locally averaged filler volume fraction.

The current approach introduces the locally averaged position-dependent filler volume density, $\bar{\phi}(x)$, into EMT, in place of a uniform value equal to the mean filler volume fraction, $\langle\phi\rangle$, or the local volume fraction $\phi(x)$ in the membrane. Thus, we use EMT to evaluate $\mathcal{D}_m\left(\bar{\phi}(x)\right)$, in which $\bar{\phi}(x)$ replaces ϕ_o in Table 1. In this way, by solving Eqs. (8)-(11) along the MMM, the calculated local MMM diffusivity depends on the particle size, membrane thickness and interfacial adsorption equilibrium. We note that the assumption that EMT holds in the end regions where the filler comprises parts of spheres is strictly not valid, as Maxwell's derivation, on which the Chiew Glandt model is based, considers the filler particles to be spherical.

However, Chang and Acrivos [34] observed this assumption to be satisfactory, while indicating that there is no formal justification for this. We do note here that at small particle size for which the effect on permeability is negligible this assumption is justifiable, but the reason for its success even at large size is essentially due to it being a correction for end effects, approximately accounting for effects of depletion of filler in this region.

3.1.3. Effective permeability

The effective MMM permeability $\left(P_m\right)$ may be estimated from the steady state flux in the membrane, upon solution of eq. (8), as:

$$P_m = \frac{\ell\left[-\mathcal{D}_m(x)\dfrac{dC_b^m}{dx}\right]}{RT\left(C_{b_1}-C_{b_2}\right)} = \frac{J_x\ell}{RT\left(-\Delta C_b\right)} \tag{25}$$

which completes the theory for the permeation of pure gases in MMMs. In summary, Eqs. (8)-(11), (20) or (22), (24) and (25), together with any of the EMT models in Table 1, comprise the proposed model to describe single gas permeation through MMM. In this initial study we consider only the low pressure region, in which the isotherms are linear, following Eqs. (13) and (14), although the theory is more general and can also accommodate nonlinear isotherms.

The above model has been solved using MATLAB®, and the results compared with the exact effective permeabilities obtained from detailed simulations are presented in the next section. The model parameters used in the present work are listed in Table 2.

Table 2. Model parameters used in calculations.

Parameter	Value(s)	SI units
$\mathcal{D}_{of}/\mathcal{D}_{oc}$	1, 10, 25, 50, 100	dimensionless
C_{b_2}	1	$\mathrm{mol/m^3}$
C_{b_1}	0	$\mathrm{mol/m^3}$
K_f/K_c	1, 10, 100	dimensionless
r_o	0.1, 1, 2, 3, 4	μm
ℓ	0–100	μm
P_f/P_c	25, 50, 100	dimensionless

3.2. Simulation

The finite element method has been implemented to solve the coupled 3d partial differential equations for the diffusive transport in both polymer and filler phases using the COMSOL Multiphysics® software package together with MATLAB®.To do so, 3d-MMMs are constructed with uniformly distributed spherical fillers with a given radius (r_o), as shown in Fig. 3 for a membrane containing particles with $r_o = 1\ \mu\text{m}$ and $\bar{\phi} = 0.1$. Initially the particles are arranged in an idealized lattice at the required mean filling fraction, and subsequently a Monte-Carlo-based algorithm is used to randomize the position of each filler particle within the simulation box, such that the particles are non-overlapping and are positioned within the simulation box without intersecting the end planes. When $\bar{\phi} \le 0.3$, the initial filler configuration is based on a simple cubic lattice, and when $\bar{\phi} > 0.3$, it is based on hexagonal-closed packed lattice. Fig. 3 illustrates typical initial and randomized final configurations as well as the corresponding positions of a tagged particle within the simulation box (coloured red).

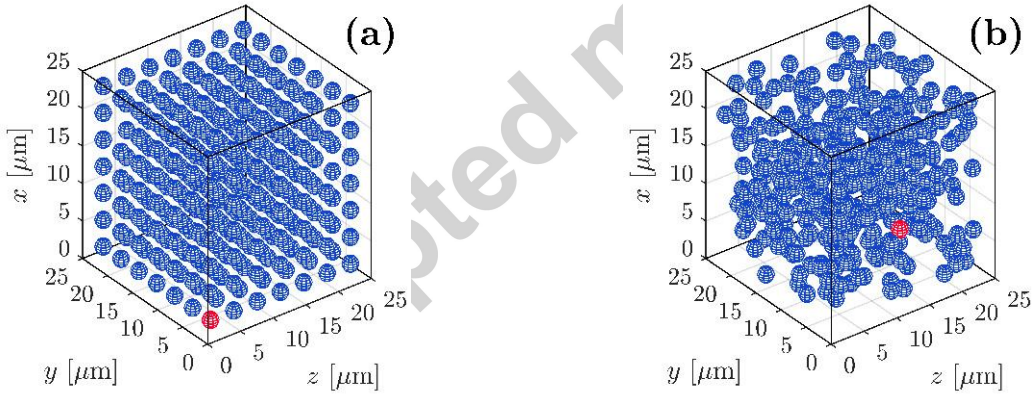

Fig. 3. Filler configuration within the MMM. (a) Initial, and (b) final configuration. Initial and final positions are illustrated for a tagged (red) particle.

Steady state transport through each phase of the composite membrane follows the continuity equation:

$$\left(-\nabla \cdot J\right) = 0 \tag{26}$$

where J is the flux through the MMM. Fick's law is used to describe the flux in the filler $\left(J_f\right)$ and matrix $\left(J_c\right)$, while considering pseudo-bulk concentration as the field variable, following

$$J_f = -\mathcal{D}_f(\nabla C_b^f) \tag{27}$$

$$J_c = -\mathcal{D}_c(\nabla C_b^c) \tag{28}$$

with $\left(\nabla C_b^f\right)$ and $\left(\nabla C_b^c\right)$ being the pseudo-bulk concentration gradients in the filler and matrix, respectively. $\mathcal{D}_f$ and are $\mathcal{D}_c$ the local diffusivities of the permeant in each phase, and follow the Darken relation in Eq. (11). In the present work, since we consider the low presure Henry law region, $\mathcal{D}_f$ and $\mathcal{D}_c$ follow Eqs. (13) and (14), respectively.

The boundary conditions, used to solve Eq. (26) are shown in Fig. 4, which is a 2d view of the filler-matrix system with a single particle. Here, equality of fluxes and pseudo-bulk concentrations are automatically set as boundary conditions at the filler-matrix interface (filler surface). Periodic boundary conditions are applied at the membrane ends in the *y* and *z* directions, as depicted in Fig. 4. Isolated system boundary conditions ($flux = 0$) at both *y* and *z* directions provide essentially identical results, as discussed subsequently. Hence, we adopted periodic boundary conditons in the bulk of the work presented here.

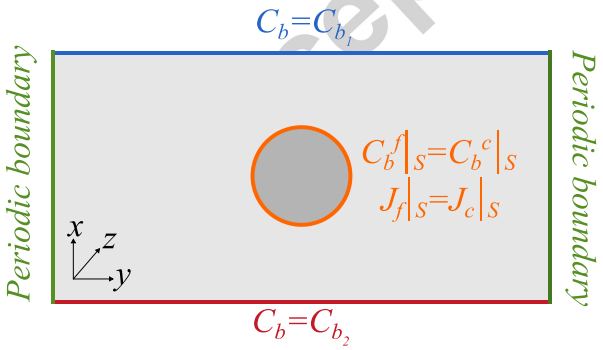

Fig. 4. Boundary conditions for Eq. (26).

A stationary fully coupled linear direct solver (MUMPS) is used to determine the numerical solutions of Eq. (26). After convergence, the numerical results are post-processed to obtain the

effective permeability of the composite membrane (P_m). To do so, the mean steady-state gas flux in the *x*-direction of each membrane is estimated as:

$$J_x = \frac{\int_{\Omega} \mathbf{n} \cdot \mathbf{J} d\Omega}{\int_{\Omega} d\Omega} = \frac{\iint_{yz} J_x(y,z) dydz}{\iint_{yz} dydz} \tag{29}$$

where Ω represents an arbitrary surface parallel to the boundaries in the *x*-direction, and $\mathbf{n}$ the corresponding normal vector. The normal flux on both *yz* surface boundaries is calculated using Eq. (29), i.e. when $x = 0$ μm and $x = 25$ μm. Once the through-flux is known, P_m is computed using Eq. (25). Here, the permeability is evaluated as the mean value computed from three independent Monte-Carlo-generated filler configurations at the corresponding filler volume fraction.

Tetrahedral meshes are used to implement the FEM, in which the maximum and minimum element sizes for a given membrane depend on the filler volume fraction. In this way, when meshing MMMs with higher filler concentrations, the MMMs is subdivided into finer elements to ensure accuracy of the simulation solution. Fig. 5 compares the permeability prediction at different volume fractions for two different meshes, in which maximum element sizes of the finer mesh are half of the ones used to build the coarser mesh. Thus, the minimum mesh density is ≈ 50 elements/μm^3 for the overall study, which corresponds to $r_o = 4$ μm and $\langle \phi \rangle = 0$,while the maximum is $\approx 2.5 \times 10^5$ elements/μm^3, which corresponds to $r_o = 0.1$ μm and $\langle \phi \rangle = 0.5$. Here, all meshes are optimized to avoid inverted elements.

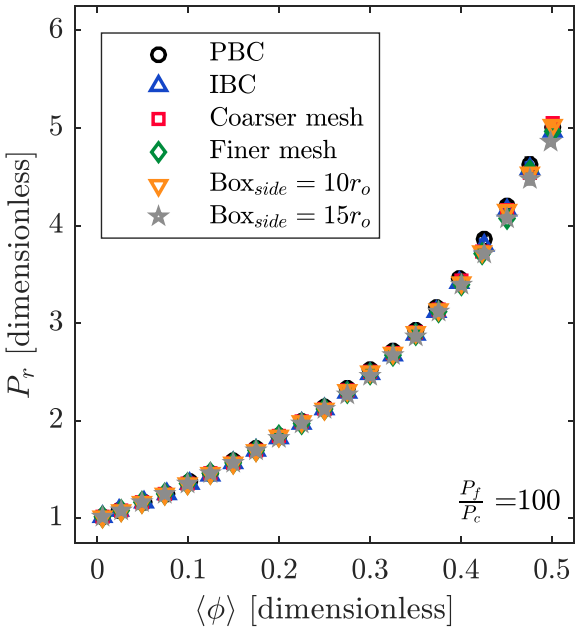

Fig. 5. Simulation convergence of MMM relative permeability for $r_o = 1$ μm with different boundary conditions, mesh density and yz box size. PBC: Periodic boundary conditions. IBC: Isolated boundary conditions. All cases yield matching results.

Each MMM is built with a fixed thickness $(\ell = 25\ \mu\text{m})$ in the *x*-direction (height) and at least 10 times the filler radius on the remaining directions (depth and width). In this way, the simulation results are independent of the box depth and width (side) as shown in Fig. 5, where the relative permeability (P_r) is compared for two different box sizes, one case corresponds to a box side of $10r_o$ and the other one to $15r_o$. The relative permeability predictions are found to be the same for both cases, demonstrating convergence.

The current approach differs from existing simulation works [5,15], because our simulations consider the gas pseudo-bulk concentration rather than its absorbed concentration as the field variable. This consideration enables automatically setting the continuity boundary at the filler-matrix interface, through equality of the pseudo-bulk concentrations and fluxes in the two phases, while in the previous works [5,15], the interfacial boundary condition for adsorption equilibrium was used (i.e. $q_f = q_c K_f / K_c$). Further, using the gas pseudo-bulk concentration as the field variable, the herein local diffusivities also denote local permeabilities, which allows direct comparison between the proposed theory and simulation predictions, as well as earlier analytical permeation models.

4. Results and discussion

4.1.1. Comparison between existing EMT-based models and exact simulations

The EMT, as commonly used, assumes that the filler particle size is small compared to the MMM thickness, so that the composite can be viewed as an effective continuum on the membrane scale [34,50]. Consequently, the models summarized in Table 1 are most appropriate for systems in which there is a large difference between the MMM thickness and dispersant size [33,66]. Accordingly, Fig. 6 depicts a comparison of results based on the existing EMT models (lines), considering uniform filler volume fraction, $\langle\phi\rangle$, and our simulations (symbols), for particle radius $r_o = 0.1\,\mu\text{m}$, which is small compared to the MMM thickness $(\ell = 25\,\mu\text{m})$. Further, we have used a value of $\phi_m = 0.637$ for the maximum filler volume fraction in the Lewis-Nielsen and Pal models, which corresponds to the random packing limit [30,35]. While all models display qualitative trends in agreement with the simulations, the Chiew-Glandt model best predicts the permeability at moderate and high filler loadings upto a filler volume fraction of 0.5. Consequently, we have adopted the Chiew-Glandt model in conjunction with our model to represent the local MMM permeability in the work described in the subsequent sections.

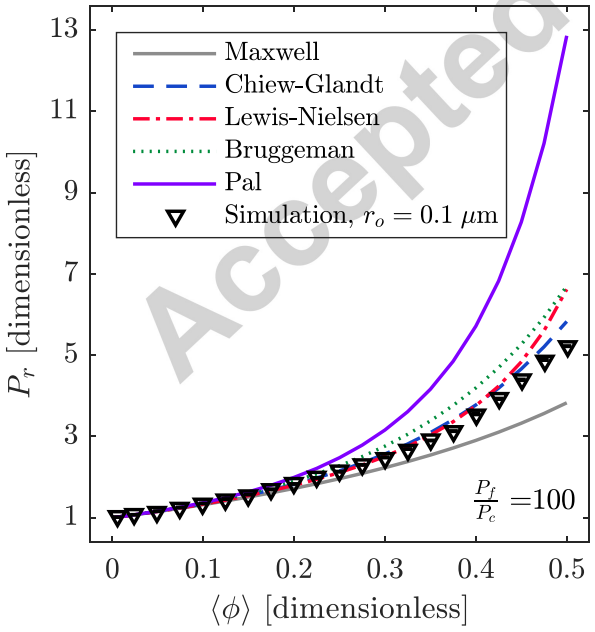

Fig. 6. Comparison between the relative permeability from conventional EMT model predictions and simulation-based results.

4.1.2. Effect of filler particle size

A key aim of this work is to establish the effect of the filler size on the effective permeability of the MMM. Fig. 7(a) depicts a comparison between the local filler volume density (continuous grey lines), $\phi(x)$, and locally averaged filler volume density (dotted color lines), $\bar{\phi}(x)$, for three particle sizes ($r_o = 0.1,\ 1,\ 4\ \mu\text{m}$) and $\phi_o = 0.5$. Here, while $\phi(x)$ gradually increases from $\phi(0) = 0$ to $\phi(r_o) = \phi_o/2 = 0.25$, the locally averaged filler volume density increases from $\bar{\phi}(0) \approx 0.03$ to $\phi(r_o) = \phi_o/2 = 0.25$. Thus, in the regions $0 < x < r_o$ and $\ell - r_o < x < \ell$ having portions of spheres with centres in $r_o \le x \le 2r_o$ and $\ell - 2r_o \le x \le \ell - r_o$, the locally averaged filler volume density is larger than the actual local filler volume density, because the regions $2r_o \le x \le 3r_o$ and $\ell - 3r_o \le x \le \ell - 2r_o$ are also sampled. The opposite effect occurs in $2r_o \le x \le 3r_o$ and $\ell - 3r_o \le x \le \ell - 2r_o$, where the local volume average also samples points in $r_o \le x \le 2r_o$ and $\ell - 2r_o \le x \le \ell - r_o$, and the local mean volume fraction is therefore smaller. The resulting local relative diffusivity profiles are depicted in Fig. 7(b), where the decrease in the local diffusivity ratio $(\mathcal{D}_m/\mathcal{D}_c)$ is seen to be consistent with that of the volume density.

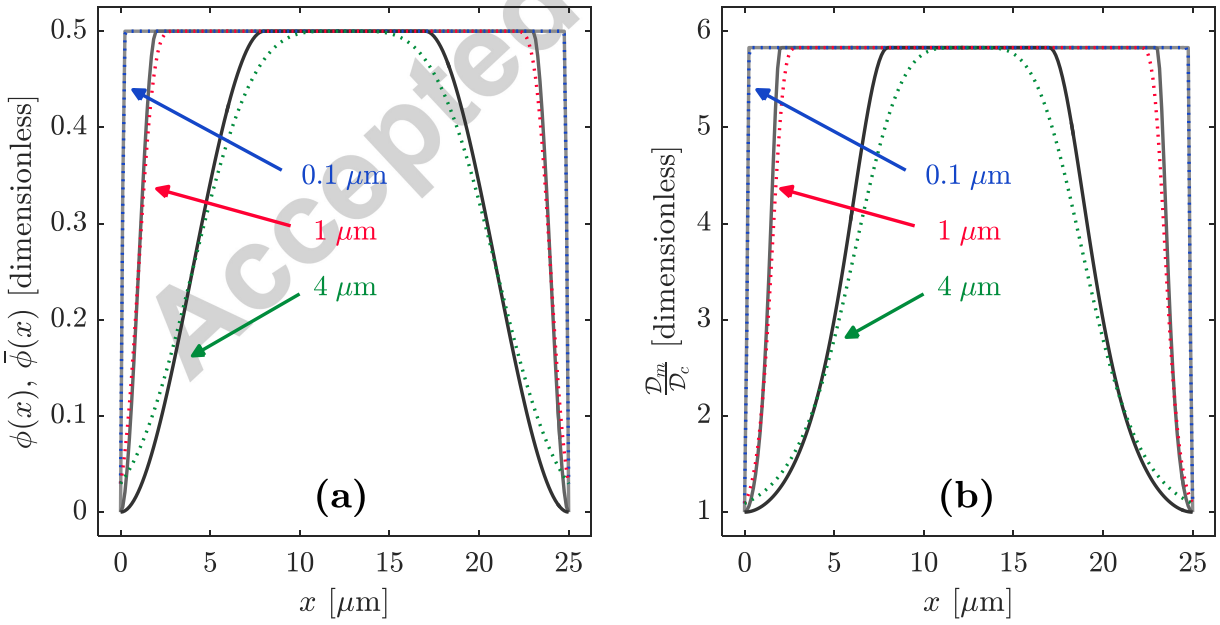

Fig. 7. Profile of the filler volume fraction and relative membrane diffusivity for $r_o = 0.1,\ 1$ and $4\ \mu\text{m}$. (a) Local and locally averaged volume fraction, and (b) local diffusivity ratio based on $\phi(x)$ (continuous grey lines) and $\bar{\phi}(x)$ (dotted coloured lines).

Fig. 8 depicts a comparison of the relative permeability predictions based on eq. (25), using the new model with both local and locally averaged volume densities, and rigorous simulation results for four different filler sizes ($r_o = 1,\ 2,\ 3$ and $4\ \mu\text{m}$), with $K_f/K_c = 1$ and $\mathcal{D}_{of}/\mathcal{D}_{oc} = 100$, so that $P_f/P_c = \mathcal{D}_f/\mathcal{D}_c = 100$. Here, the theory predictions are also compared to the Chiew-Glandt model (grey continuous line) with uniform filler volume fraction equal to $\langle\phi\rangle$, which matches the exact solution when small particles are considered (c.f. Fig. 6). In Fig. 8(a) and (b), the Chiew-Glandt model is only able to match the simulation predictions at low filler loadings $\left(\langle\phi\rangle \le 0.25\right)$ for all particle sizes. Further, in Fig. 8(a), in which the local filler volume fraction $\phi(x)$ is used, the permeability predictions for $r_o = 2\ \mu\text{m}$ and $r_o = 4\ \mu\text{m}$ slighly deviate from the simulation results (error within about 10%) at filler volume fractions exceeding about 0.4. Such deviations are alleviated and the prediction error reduced to within 3% upon using the locally averaged filler volume fraction in the model, as seen in Fig. 8(b). Here, both simulation and theory show that increase of filler particle size decreases the effective relative permeability. Such deterioration in performance may be associated with decrease of the specific polymer-filler interfacial area as the particle size increases [15,19]. Further, the number of particles per unit volume increases with decrease of the filler size, at fixed filler volume fraction. Thus, because the overall filler surface area then increases, there is more potential polymer-filler interfacial area in MMMs containing smaller particles at a given filler volume fraction.

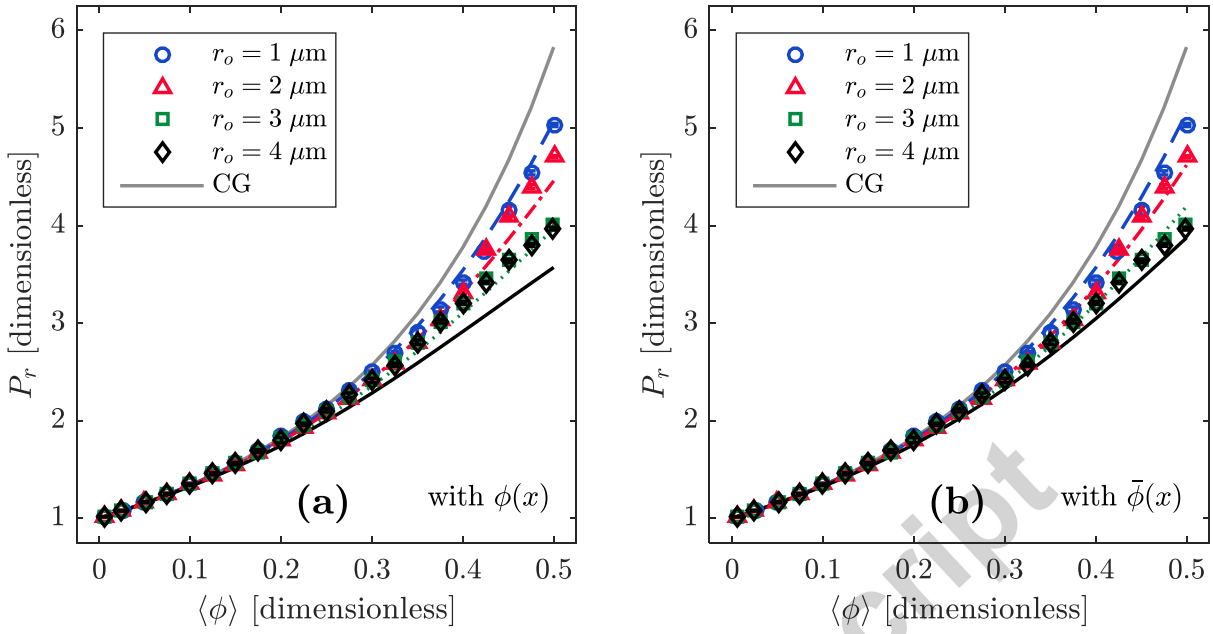

Fig. 8. Effect of the filler size on relative MMM permeability for $K_f/K_c = 1$ and $\mathcal{D}_{of}/\mathcal{D}_{oc} = 100$, for which $P_f/P_c = \mathcal{D}_f/\mathcal{D}_c = 100$, (a) using the local filler volume density, and (b) using the locally averaged filler volume density in EMT. Symbols represent exact simulation results, and lines the corresponding results from current theory. CG: Original Chiew-Glandt model, providing predictions equivalent to those of the new model with $r_o \to 0$.

The current predictions demonstrate considerable improvement compared to using the Chiew-Glandt model with constant filler volume fraction. Here, the error of the proposed model is about 10% at $\langle\phi\rangle = 0.5$ when using the local filler volume fraction to estimate the local relative diffusivity, and 3% at $\langle\phi\rangle = 0.5$ when using the locally averaged filler volume fraction, while for the original Chiew-Glandt model it is approximately 40% at the same mean filler volume fraction. The small difference between our theory and simulations occurs because the system increasingly deviates from an effective continuum when large particles are placed in the MMM. We notice that while the current model accounts for the effect of particle size through the volume averaged filler volume density profile this is essentialy an end effect correction in finite sized systems, and does not completely overcome the increased departure from an effective contimuum at particle sizes that are not negligible in comparison to the membrane thickness. Thus, for example, when $r_o = 4\ \mu$m, only three particles can be placed along the membrane thickness $(25\ \mu\text{m})$, and local packing effects of the filler become significant, leading to deviation of the continuum assumption. This behaviour is illustrated in Fig. 9, which depicts a

comparison of the pseudo-bulk concentration profile at $\langle\phi\rangle = 0.1$ and $\langle\phi\rangle = 0.5$ when $r_o = 4$ μm for both simulation and theory. Here, theoretical pseudo-bulk concentration profiles with the local (black continuous lines) and locally averaged (red dotted lines) volume density are also depicted in Fig. 9. For the simulation, the pseudo-bulk concentration profile is averaged on the yz plane at any position x in the direction of flow, while also calculating the mean value for three different random configurations.

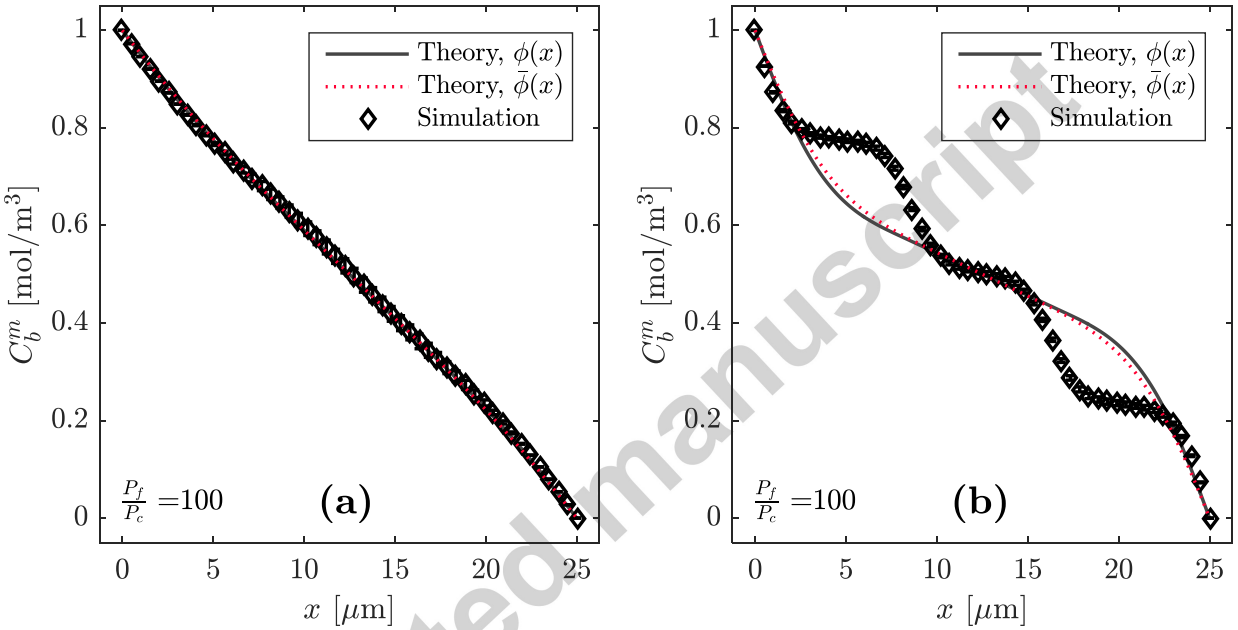

Fig. 9. Comparison between the theoretical and simulation-based pseudo-bulk concentration profiles with $P_f/P_c = \mathcal{D}_f/\mathcal{D}_c = 100$, for (a) $\langle\phi\rangle = 0.1$, and (b) $\langle\phi\rangle = 0.5$, for $r_o = 4$ μm and membrane thickness $\ell = 25$ μm.

In Fig. 9(a) and (b), a steeper pseudo-bulk concentration profile is evident close to both membrane ends ($x = 0$ μm and $x = 25$ μm), which is due to the increased volume density of the polymer phase, arising from depletion of the lower resistance filler phase, in these regions. While the theory predictions match the simulation results at low filler loadings, as seen in Fig. 9(a), and at high filler concentration in Fig. 9(b), the simulation predictions show a systematic sinusoidal variation in curvature that is absent in the theoretical predictions. Such curvature changes in the simuation-based pseudo-bulk concentration profile in Fig. 9(b) occur because the gas is only permeating through three particles along membrane thickness, as shown in Fig. 10, so that the concentration profile reflects the'grainy' texture of the membrane arising from layering effects in

the filler packing. Fig. 10(a) depicts the 3d pseudo-bulk concentration profile for $r_o = 4$ μm and $\langle\phi\rangle = 0.5$ while the 2d profile on the *x*-*y* plane for a slice placed at $z = 50$ μm is shown in Fig. 10(b), both illustrating the 'grainy' texture of the composite.

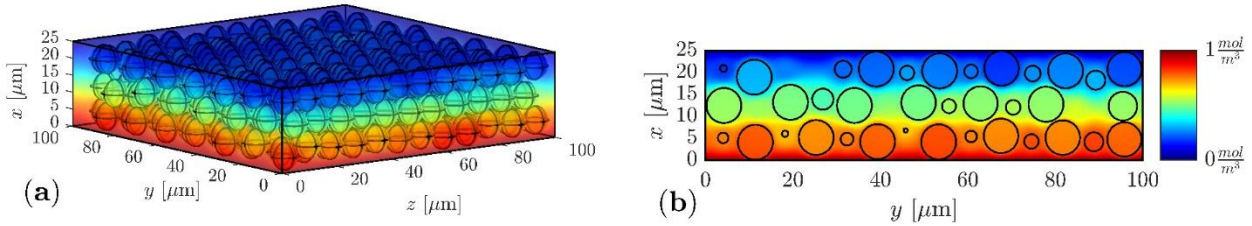

Fig. 10. Simulation-based pseudo-bulk concentration profile with $P_f/P_c = \mathcal{D}_f/\mathcal{D}_c = 100$ and $\langle\phi\rangle = 0.5$, depicted in a (a) 3d view, and (b) 2d view on a xy-slice placed at $z = 50$ μm, for $r_o = 4$ μm and membrane thickness $\ell = 25$ μm.

4.1.3. Effect of the membrane thickness

The dependence of relative permeability on the the membrane thickness has also been studied. Fig. 11 depicts the theoretical variation of the relative permeability with membrane thickness for various particle sizes at fixed nominal filler volume fraction $(\phi_o = 0.5)$, with $K_f/K_c = 1$ and $\mathcal{D}_{of}/\mathcal{D}_{oc} = 100$, so that $P_f/P_c = \mathcal{D}_f/\mathcal{D}_c = 100$. Here, the model uses the locally averaged volume fraction in the local diffusivity calculation. Based on the new model, the permeability is a function of the ratio of the filler size to the membrane thickness (r_o/ℓ), and therefore increase with membrane thickness at fixed particle size is analogous to decreasing the filler particle size at fixed membrane thickness. Consequntly, the relative permeability increases with the increase of the membrane thickness for all particle sizes in Fig. 11, which is consistent with the results presented above, showing increase in permeability with decrease in particle radius. Further, in Fig. 11, the relative permeability is equal to unity for membrane in which $\ell \le 2r_o$, since we take $\phi(x) = 0$ when $\ell \le 2r_o$. For membranes in which $\ell > 2r_o$, the permeability gradually increases and asymptotically approaches the result from the conventional EMT, which applies to an infinite continuum. Such behavior can be seen from the permeability profiles for $r_o = 0.01$ μm (grey continuous line) and $r_o = 0.1$ μm (blue dashed line).

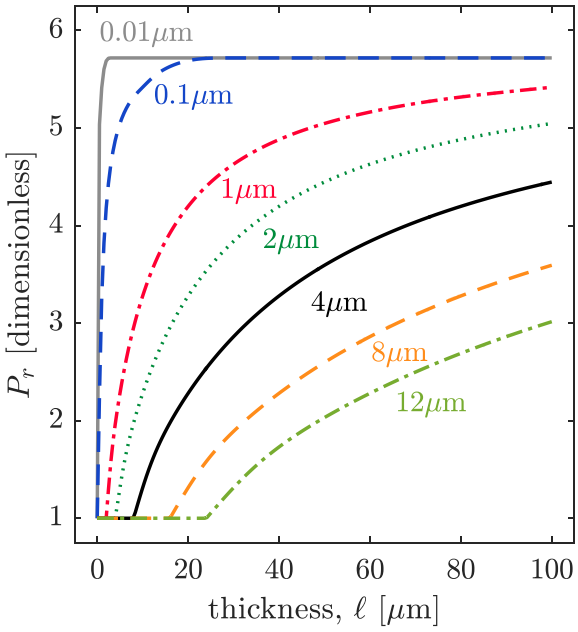

Fig. 11. Dependence of relative permeability on membrane thickness, for $\phi_o = 0.5$, $P_f/P_c = \mathcal{D}_f/\mathcal{D}_c = 100$ and various values of r_o.

4.1.4. Effect of the filler-to-matrix permeability ratio

It is well known that the effective permeability increases with increase of the filler-to-matrix permeability ratio P_f/P_c [12,25,51]. Fig. 12 depicts a comparison of the effective relative permeability predicted by the present model and simulations for different filler sizes ($r_o = 1$, 2, 3 and $4\mu m$) for two filler-to-matrix permeability ratios. Here, $K_f/K_c = 1$ for all cases, while $\mathcal{D}_{of}/\mathcal{D}_{oc} = 25$ and $\mathcal{D}_{of}/\mathcal{D}_{oc} = 50$, for $P_f/P_c = \mathcal{D}_f/\mathcal{D}_c = 25$ and $P_f/P_c = \mathcal{D}_f/\mathcal{D}_c = 50$, respectively. Comparing the relative permeability profiles in Fig. 12(a) and (b), it is seen that increase of the filler-to-matrix permeability ratio favours MMM performance, as expected. Further, the decrease of the relative permeability with increase of filler particle size is greater for $P_f/P_c = \mathcal{D}_f/\mathcal{D}_c = 50$ than when $P_f/P_c = \mathcal{D}_f/\mathcal{D}_c = 25$, for both model and simulation.

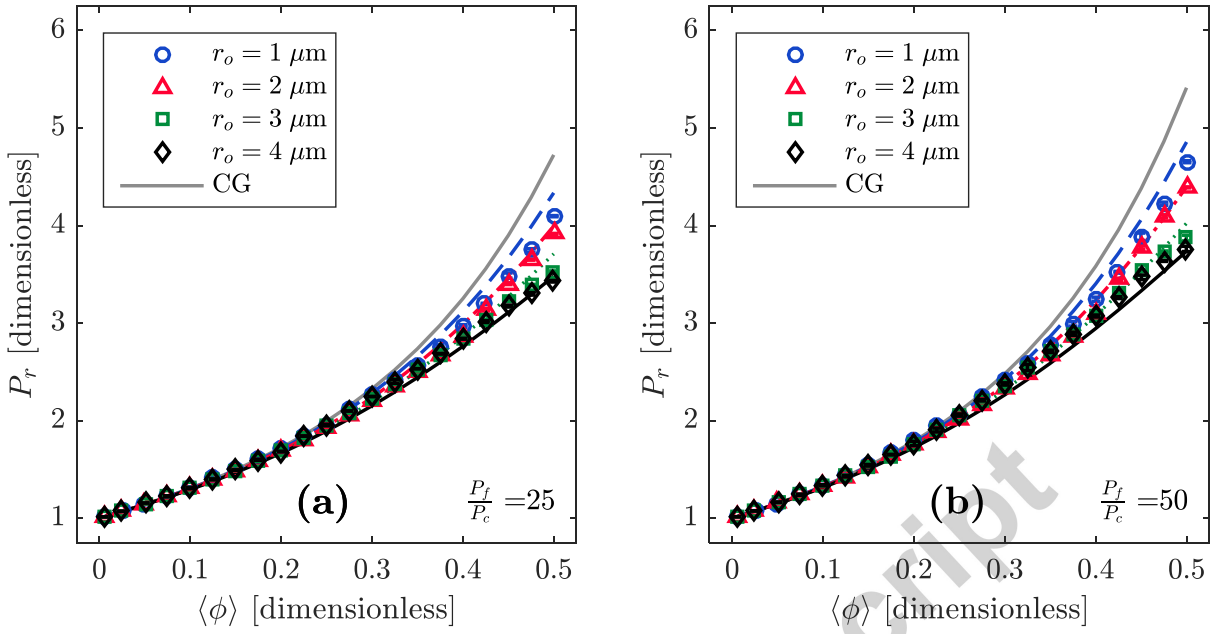

Fig. 12. Comparison of the theoretical and exact relative permeability profiles at various filler sizes, and different filler-to-matrix permeability ratios. (a) $P_f/P_c = \mathcal{D}_f/\mathcal{D}_c = 25$, and (b) $P_f/P_c = \mathcal{D}_f/\mathcal{D}_c = 50$. Symbols represent exact simulation results, and lines the corresponding results from current theory. CG: Original Chiew-Glandt model, providing predictions equivalent to those of the new model with $r_o \to 0$.

It is evident from Fig. 8(b) and Fig. 12 that the error of the theory increases slightly at high filler volume fractions, and when large particles are placed within the MMM. Such reduction in accuracy is expected, because the transport through the MMM is significantly affected by the filler intrinsic properties. Thus, when $P_f / P_c \gg 1$, the heterogeneous medium may no longer be accurately mapped into an effective homogeneous one at particle sizes not much smaller than the membrane thickness. Nevertheless, the theory deviates only very marginally from the exact calculations even when r_o is as large as 4 μm, and the error is only about 3% for $P_f/P_c = 100$, 2% for $P_f/P_c = 50$ and 1% for $P_f/P_c = 25$ at $\langle\phi\rangle = 0.5$.

4.1.5. Effect of the filler-to-matrix diffusivity and equilibrium constant ratios

Previous simulations have suggested that different combinations of K_f/K_c and $\mathcal{D}_{of}/\mathcal{D}_{oc}$, while keeping $P_f/P_c = \mathcal{D}_f/\mathcal{D}_c = K_f\mathcal{D}_{of}/K_c\mathcal{D}_{oc}$ constant, yield different effective permeability values [5,15]. This is inconsistent with conventional effective medium theory, various versions

of which are presented in Table 1, as well as with the current theory, which yield the permeability of the composite (P_m or $\mathcal{D}_m$) based on the ratio of permeabilities of the filler (P_f or $\mathcal{D}_f$) and of the polymer matrix (P_c or $\mathcal{D}_c$). It may be seen from from Eqs. (13), (14) and (30), (31) that the products $K_f\mathcal{D}_{of}$ and $K_c\mathcal{D}_{oc}$ provide the overall filler $\left(\mathcal{D}_f\right)$ and matrix $\left(\mathcal{D}_c\right)$ diffusivity values for both simulation and theory, and therefore no difference should be found if their ratio is held constant. To confirm this, a comparison between the model predictions and exact simulation-based calculations is made in Fig. 13 with $K_f/K_c = 1,\ 10,\ 100$ and $\mathcal{D}_{of}/\mathcal{D}_{oc} = 100,\ 10,\ 1$ with $P_f/P_c = \mathcal{D}_f/\mathcal{D}_c = 100$ in all cases. No difference is found between the relative permeability predictions of the simulation for all combinations, consistent with the theory.

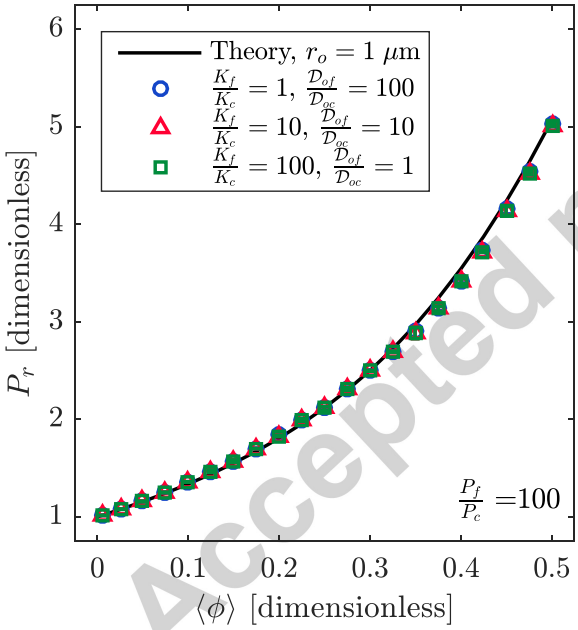

Fig. 13. Effect of different combinations of the filler-to-matrix diffusivity and equilibrium constant ratios, at constant filler to matrix permeability ratio, on the relative effective permeability of the mixed matrix membrane.

4.1.6. Effect of packing structure

Can variations in packing structure of the filler affect the overall permability of the composite and, if so, what is the most favourable structure? While in practice one expects the random structure to be the one approached experimentally, with the advent of 3d printing it may become

possible to synthesise MMMs with any specified filler packing structure in the future. The effect of the packing configuration has therefore been investigatied in this work. To this end, 3d-MMMs were built with filler particles located in simple cubic (SC), random, body-centered cubic (BCC), face-centered cubic (FCC) and hexagonal-closed packed (HCP) lattices. Examples of the three filler configurations for $r_o = 1\ \mu\text{m}$ and $\langle\phi\rangle = 0.1$ are depicted in Fig. 14.

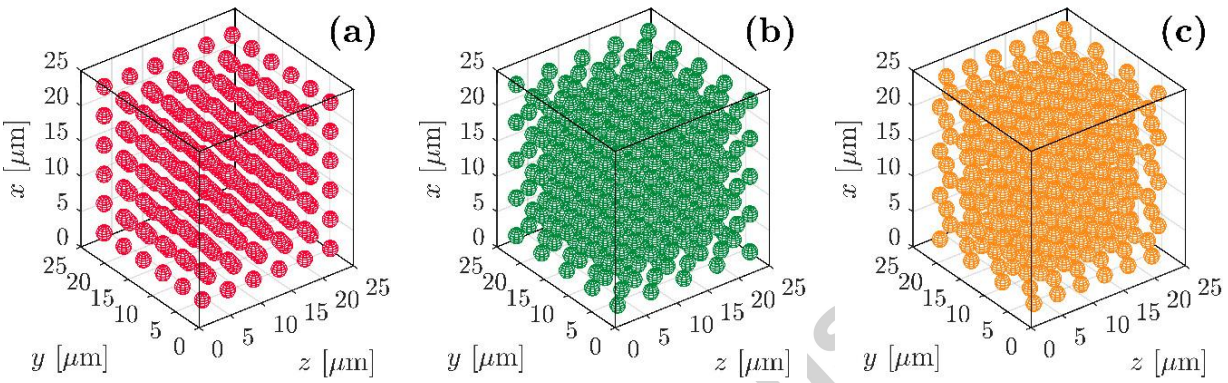

Fig. 14. Packing structures for $r_o = 1\ \mu\text{m}$ and $\langle\phi\rangle = 0.1$. (a) Body-centred cubic (BCC), (b) face-centred cubic (FCC), and (c) hexagonal-closed packed (HCP) lattices.

The exact effective permeabilities have been determined for all configurations following the simulation methodology described in Section 3.2, and Fig. 15 compares the simulation results for all cases. No apparent improvement on the effective permeability is achieved with change in the packing configuration. At low filler concentrations $\left(\langle\phi\rangle < 0.2\right)$, all packing configurations provide the same prediction of the relative permeability. At moderate filler loadings $\left(0.2 \le \langle\phi\rangle \le 0.4\right)$, all configurations provide slightly smaller relative permeability predictions compared to random packing. Finally, at high particle concentrations $\left(0.4 < \langle\phi\rangle \le 0.5\right)$, the simple cubic lattice provides nearly the same prediction as the random configuration. Such behavior suggests that the regular filler packing configurations (BCC, FCC, HCP) may lead to reduced permeabilities because the gas molecules follow the paths of least resistance, avoiding the uninterrupted low permeability paths in the space occupied by the polymer matrix adjacent to the filler particles. Hence, the relative permeability of these structures is lower compared to the

random structure at high filler volume fractions, as the gas molecules follow the higher permability paths through the particles. However, further studies should be carried out in order to comfirm this.

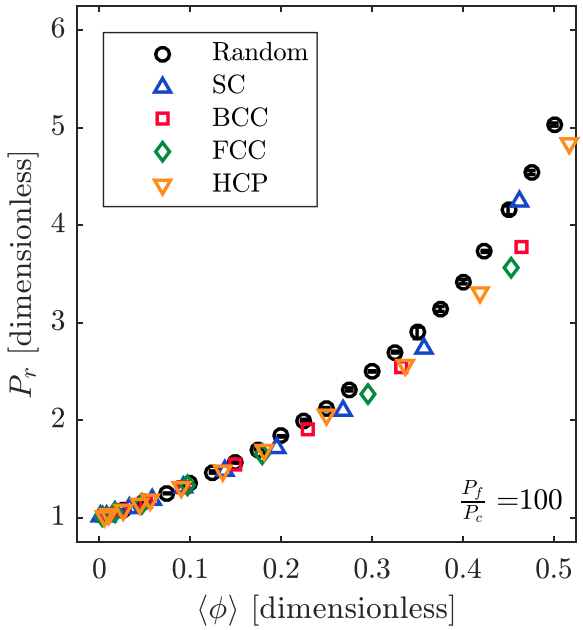

Fig. 15. Exact simulation-based results for the relative permeability for different packing configurations, with $P_f/P_c = \mathcal{D}_f/\mathcal{D}_c = 100$.

5. Conclusions

This work has presented a new theory for the permeation of pure gases in flat mixed-matrix membranes, considering nonuniformity of the filler fraction in finite sized membranes. The mixed-matrix membrane flux, estimated through EMT, satisfies the transport equation for the composite, while using a position-dependent local permeability (diffusivity); this leads the MMM permeability to be dependent on the filler particle size and the membrane thickness. In this way, both EMT and transport models are coupled in a self-consistent manner, which is key to obtaining the MMM permeability while accounting for the finite filler particle size, and overcoming the assumption of the uniformity of the field, inherent to existing theories of transport in composite media. The pedictions of the theory have been validated against exact simulation-based results, showing excellent agreement.

A decrease of the effective permeability is found with increase of the particle size, which is associated with the decrease of the specific polymer-filler interfacial area. Here, both theory

predictions and exact calculations are in very good agreement, with differences less than about 3-5% at large filler volume fractions. Further, no difference is found in the exact relative permeability when altering the filler-to-matrix equilibrium constants and filler-to-matrix intrinsic diffusivities at constant filler-to-matrix permeability ratio, which is consistent with the proposed theory. Finally, very little relative permeability difference is found with changes in the filler packing configuration, with the random structure being the most favourable and showing a slightly higher effective permeability compared to the regular structures. This is due to the filler particles offering higher permeability pathways compared to the continuous polymer-filled regions adjacent to the particles in the regular structures.

Acknowledgement

This work has been supported by a grant (No. DP150101996) from the Australian Research Council, through the Discovery scheme.

References

[1] C. Liu, S. Kulprathipanja, Mixed-Matrix Membranes, in: Zeolites Ind. Sep. Catal., Wiley-VCH Verlag GmbH & Co. KGaA, 2010: pp. 329–353.

[2] M.A. Aroon, A.F. Ismail, T. Matsuura, M.M. Montazer-Rahmati, Performance studies of mixed matrix membranes for gas separation: A review, Sep. Purif. Technol. 75 (2010) 229–242.

[3] A.F. Ismail, K.C. Khulbe, T. Matsuura, Gas separation membranes: Polymeric and inorganic, 2015.

[4] D. Bastani, N. Esmaeili, M. Asadollahi, Polymeric mixed matrix membranes containing zeolites as a filler for gas separation applications: A review, J. Ind. Eng. Chem. 19 (2013) 375–393.

[5] T. Singh, D.-Y. Kang, S. Nair, Rigorous calculations of permeation in mixed-matrix membranes: Evaluation of interfacial equilibrium effects and permeability-based models, J. Memb. Sci. 448 (2013) 160–169.

[6] H. Vinh-Thang, S. Kaliaguine, Predictive Models for Mixed-Matrix Membrane Performance: A Review, Chem. Rev. 113 (2013) 4980–5028.

[7] L.M. Robeson, The upper bound revisited, J. Memb. Sci. 320 (2008) 390–400.

[8] S. Basu, A. Cano-Odena, I.F.J. Vankelecom, MOF-containing mixed-matrix membranes for CO2/CH4 and CO2/N2 binary gas mixture separations, Sep. Purif. Technol. 81 (2011) 31–40.

[9] S.A. Hashemifard, A.F. Ismail, T. Matsuura, Prediction of gas permeability in mixed matrix membranes using theoretical models, J. Memb. Sci. 347 (2010) 53–61.

[10] D. Hua, Y.K. Ong, Y. Wang, T. Yang, T.-S. Chung, ZIF-90/P84 mixed matrix membranes for pervaporation dehydration of isopropanol, J. Memb. Sci. 453 (2014) 155–167.

[11] H. Fan, Q. Shi, H. Yan, S. Ji, J. Dong, G. Zhang, Simultaneous Spray Self-Assembly of Highly Loaded ZIF-8–PDMS Nanohybrid Membranes Exhibiting Exceptionally High Biobutanol-Permselective Pervaporation, Angew. Chemie Int. Ed. 53 (2014) 5578–5582.

[12] H. Vinh-Thang, S. Kaliaguine, A comprehensive computational strategy for fitting experimental permeation data of mixed matrix membranes, J. Memb. Sci. 452 (2014) 271–276.

[13] T.-S. Chung, L.Y. Jiang, Y. Li, S. Kulprathipanja, Mixed matrix membranes (MMMs)

comprising organic polymers with dispersed inorganic fillers for gas separation, Prog. Polym. Sci. 32 (2007) 483–507.

[14] H.B. Tanh Jeazet, C. Staudt, C. Janiak, Metal-organic frameworks in mixed-matrix membranes for gas separation, Dalt. Trans. 41 (2012) 14003–14027.

[15] A.-C. Yang, C.-H. Liu, D.-Y. Kang, Estimations of effective diffusivity of hollow fiber mixed matrix membranes, J. Memb. Sci. 495 (2015) 269–275.

[16] Y. Shen, A.C. Lua, Theoretical and experimental studies on the gas transport properties of mixed matrix membranes based on polyvinylidene fluoride, AIChE J. 59 (2013) 4715–4726.

[17] B. Shimekit, H. Mukhtar, T. Murugesan, Prediction of the relative permeability of gases in mixed matrix membranes, J. Memb. Sci. 373 (2011) 152–159.

[18] M. Rezakazemi, A. Ebadi Amooghin, M.M. Montazer-Rahmati, A.F. Ismail, T. Matsuura, State-of-the-art membrane based CO2 separation using mixed matrix membranes (MMMs): An overview on current status and future directions, Prog. Polym. Sci. 39 (2014) 817–861.

[19] A.L. Andrady, T.C. Merkel, L.G. Toy, Effect of Particle Size on Gas Permeability of Filled Superglassy Polymers, Macromolecules. 37 (2004) 4329–4331.

[20] J. Li, J. Shao, Q. Ge, G. Wang, Z. Wang, Y. Yan, Influences of the zeolite loading and particle size in composite hollow fiber supports on properties of zeolite NaA membranes, Microporous Mesoporous Mater. 160 (2012) 10–17.

[21] Ş.B. Tantekin-Ersolmaz, Ç. Atalay-Oral, M. Tatlıer, A. Erdem-Şenatalar, B. Schoeman, J. Sterte, Effect of zeolite particle size on the performance of polymer–zeolite mixed matrix membranes, J. Memb. Sci. 175 (2000) 285–288.

[22] J.D. Felske, Effective thermal conductivity of composite spheres in a continuous medium with contact resistance, Int. J. Heat Mass Transf. 47 (2004) 3453–3461.

[23] Y.C. Chiew, E.D. Glandt, The effect of structure on the conductivity of a dispersion, J. Colloid Interface Sci. 94 (1983) 90–104.

[24] D.J. Jeffrey, Conduction Through a Random Suspension of Spheres, Proc. R. Soc. London A Math. Phys. Eng. Sci. 335 (1973) 355–367.

[25] R. Pal, New models for thermal conductivity of particulate composites, J. Reinf. Plast. Compos. 26 (2007) 643–651.

[26] J.C. Maxwell, A treatise on electricity and magnetism, Clarendon Press, Oxford, 1873.

[27] R. Pal, On the Lewis–Nielsen model for thermal/electrical conductivity of composites, Compos. Part A Appl. Sci. Manuf. 39 (2008) 718–726.

[28] L.E. Nielsen, Thermal conductivity of particulate-filled polymers, J. Appl. Polym. Sci. 17 (1973) 3819–3820.

[29] L.E. Nielsen, The Thermal and Electrical Conductivity of Two-Phase Systems, Ind. Eng. Chem. Fundam. 13 (1974) 17–20.

[30] R. Pal, Permeation models for mixed matrix membranes, J. Colloid Interface Sci. 317 (2008) 191–198.

[31] H.T. Davis, The Effective Medium Theory of Diffusion in Composite Media, J. Am. Ceram. Soc. 60 (1977) 499–501.

[32] E. Marand, A. Surapathi, The role of solubility partition coefficient at the mixed matrix interface in the performance of mixed matrix membranes, J. Memb. Sci. 415–416 (2012) 871–877.

[33] E.Y. Chang, A. Acrivos, Conduction of heat from a planar wall with uniform surface temperature to a monodispersed suspension of spheres, J. Appl. Phys. 62 (1987) 771-776.

[34] E. Chang, A. Acrivos, Rate of heat conduction from a heated sphere to a matrix containing passive spheres of a different conductivity, J. Appl. Phys. 59 (1986) 3375-3382.

[35] E. Gonzo, M. Parentis, J. Gottifredi, Estimating models for predicting effective permeability of mixed matrix membranes, J. Memb. Sci. 277 (2006) 46–54.

[36] S.A. Hashemifard, A.F. Ismail, T. Matsuura, A new theoretical gas permeability model using resistance modeling for mixed matrix membrane systems, J. Memb. Sci. 350 (2010) 259–268.

[37] D.-Y. Kang, C.W. Jones, S. Nair, Modeling molecular transport in composite membranes with tubular fillers, J. Memb. Sci. 381 (2011) 50–63. doi:10.1016/j.memsci.2011.07.015.

[38] T.B. Lewis, L.E. Nielsen, Dynamic mechanical properties of particulate-filled composites, J. Appl. Polym. Sci. 14 (1970) 1449–1471.

[39] J.H. Petropoulos, A comparative study of approaches applied to the permeability of binary composite polymeric materials, J. Polym. Sci. Polym. Phys. Ed. 23 (1985) 1309–1324.

[40] H.T. Davis, L.R. Valencourt, C.E. Johnson, Transport Processes in Composite Media, J. Am. Ceram. Soc. 58 (1975) 446–452.

[41] A.G. Every, Y. Tzou, D.P.H. Hasselman, R. Raj, The effect of particle size on the thermal conductivity of ZnS/diamond composites, Acta Metall. Mater. 40 (1992) 123–129.

[42] D.J. Jeffrey, Group Expansions for the Bulk Properties of a Statistically Homogeneous, Random Suspension, Proc. R. Soc. London A Math. Phys. Eng. Sci. 338 (1974) 503–516.

[43] Y.C. Chiew, E.D. Glandt, Effective conductivity of dispersions: The effect of resistance at the particle surfaces, Chem. Eng. Sci. 42 (1987) 2677–2685.

[44] D.A.G. Bruggeman, Berechnung verschiedener physikalischer Konstanten von heterogenen Substanzen, Ann. Phys. 24 (1935) 636.

[45] Z. Hashin, Assessment of the Self Consistent Scheme Approximation: Conductivity of Particulate Composites, J. Compos. Mater. . 2 (1968) 284–300.

[46] S. Rafiq, A. Maulud, Z. Man, M.I.A. Mutalib, F. Ahmad, A.U. Khan, A.L. Khan, M. Ghauri, N. Muhammad, Modelling in mixed matrix membranes for gas separation, Can. J. Chem. Eng. 93 (2015) 88–95.

[47] S.-Y. Lu, S. Kim, Effective thermal conductivity of composites containing spheroidal inclusions, AIChE J. 36 (1990) 927–938.

[48] Z. Sadeghi, M. Omidkhah, M.E. Masoumi, R. Abedini, Modification of existing permeation models of mixed matrix membranes filled with porous particles for gas separation, Can. J. Chem. Eng. 94 (2016) 547–555.

[49] J.C. Halpin Affdl, J.L. Kardos, The Halpin-Tsai equations: A review, Polym. Eng. Sci. 16 (1976) 344–352.

[50] J. Ordóñez-Miranda, J.J. Alvarado-Gil, R. Medina-Ezquivel, Generalized Bruggeman Formula for the Effective Thermal Conductivity of Particulate Composites with an Interface Layer, Int. J. Thermophys. 31 (2010) 975–986.

[51] R.H.B. Bouma, A. Checchetti, G. Chidichimo, E. Drioli, Permeation through a heterogeneous membrane: the effect of the dispersed phase, J. Memb. Sci. 128 (1997) 141–149.

[52] T.T. Moore, W.J. Koros, Gas sorption in polymers, molecular sieves, and mixed matrix membranes, J. Appl. Polym. Sci. 104 (2007) 4053–4059.

[53] R. Mahajan, W.J. Koros, Mixed matrix membrane materials with glassy polymers. Part 1, Polym. Eng. Sci. 42 (2002) 1420–1431.

[54] C.M. Zimmerman, A. Singh, W.J. Koros, Tailoring mixed matrix composite membranes

for gas separations, J. Memb. Sci. 137 (1997) 145–154.

[55] T. Wang, D.-Y. Kang, Highly selective mixed-matrix membranes with layered fillers for molecular separation, J. Memb. Sci. 497 (2015) 394–401.

[56] T. Wang, D.-Y. Kang, Predictions of effective diffusivity of mixed matrix membranes with tubular fillers, J. Memb. Sci. 485 (2015) 123–131.

[57] M. Minelli, M.G. Baschetti, F. Doghieri, A comprehensive model for mass transport properties in nanocomposites, J. Memb. Sci. 381 (2011) 10–20.

[58] B. Seoane, J. Coronas, I. Gascon, M.E. Benavides, O. Karvan, J. Caro, F. Kapteijn, J. Gascon, Metal-organic framework based mixed matrix membranes: a solution for highly efficient CO2 capture?, Chem. Soc. Rev. 44 (2015) 2421–2454.

[59] E.J.F. Dickinson, H. Ekström, E. Fontes, COMSOL Multiphysics®: Finite element software for electrochemical analysis. A mini-review, Electrochem. Commun. 40 (2014) 71–74.

[60] D.M. Ruthven, Principles of adsorption and adsorption processes, John Wiley & Sons, 1984.

[61] J. Kärger, Some remarks on the straight and cross-coefficients in irreversible thermodynamics of surface flow and on the relation between diffusion and selfdiffusion, Surf. Sci. 36 (1973) 797–801.

[62] I. Bitsanis, T.K. Vanderlick, M. Tirrell, H.T. Davis, A tractable molecular theory of flow in strongly inhomogeneous fluids, J. Chem. Phys. 89 (1988) 3152-3162.

[63] I. Bitsanis, J.J. Magda, M. Tirrell, H.T. Davis, Molecular dynamics of flow in micropores, J. Chem. Phys. 87 (1987) 1733-1750.

[64] S.K. Bhatia, D. Nicholson, Modeling Mixture Transport at the Nanoscale: Departure from Existing Paradigms, Phys. Rev. Lett. 100 (2008) 236103.

[65] S.K. Bhatia, D. Nicholson, Transport of simple fluids in nanopores: Theory and simulation, AIChE J. 52 (2006) 29–38.

[66] A. Acrivos, E. Chang, A model for estimating transport quantities in two-phase materials, Phys. Fluids. 29 (1986) 3-4.

Highlights

- Filler volume fraction is non-uniform in finite sized composite membranes
- Effective medium theory is extended to finite systems
- The theory is in remarkable agreement with detailed simulations
- Membrane permeability decreases on increasing particle size.
- Filler packing structure only weakly affects permeability of the composite.